Estimation of Fluorescence Lifetimes via Rotational Invariance Techniques

Estimation of Fluorescence Lifetimes via Rotational Invariance Techniques

Hongqi Yu*, Rebecca Saleeb, Paul Dalgarno, and David Day-Uei Li$

***Abstract*—Estimation of signal parameters via rotational invariance techniques is a classical algorithm widely used in array signal processing for direction-of-arrival estimation of emitters. Inspired by this method, a new signal model and a new fluorescence lifetime estimation via rotational invariance techniques (FLERIT) were developed for multi-exponential fluorescence lifetime imaging (FLIM) experiments. The FLERIT only requires a few time bins of a histogram generated by a time-correlated single photon counting FLIM system, greatly reducing the data throughput from the imager to the signal processing units. As a non-iterative method, the FLERIT does not require initial conditions, prior information nor model selection that are usually required by widely used traditional fitting methods, including nonlinear least square methods or maximum likelihood methods. Moreover, its simplicity means it is suitable for implementations in embedded systems for real-time applications. FLERIT was tested on synthesized and experimental fluorescent cell data showing the potentials to be widely applied in FLIM data analysis.**

***Index Terms*—Fluorescence microscopy, fluorescence lifetime imaging microscopy (FLIM), time-correlated single photon counting (TCSPC), time-resolved imaging.**

I. Introduction

FLUORESCENCE lifetime imaging (FLIM) is a powerful tool to study the micro-structure and micro-environments of molecules. FLIM has been widely used throughout modern microscopy, including in the material sciences, biology, chemical analysis and even for clinical diagnosis. Different from traditional fluorescence intensity imaging, which only provides geometric information of tissues or materials, FLIM measures the inherent lifetime of a fluorescent molecule (fluorophore) as it undergoes radiative absorption and subsequent fluorescent relaxation. As the fluorescence lifetime is sensitive to the environment, FLIM can be a good indicator to show how the fluorophore interacts with its microenvironment. Examples include imaging physiological or electrochemical parameters such as Ca^{2+}, pH and pO2 [1-5]. When combined with fluorescence resonance energy transfer (FRET)[6-8] FLIM is the most robust method to study protein-protein interactions [1, 2], premalignant lesions [3], molecular metabolism [4] and drug-targeting efficacy [5]. However, despite the potential and significant impact of FLIM, primarily in the biological sciences, estimation of the fluorescence lifetimes remains a significant challenge, particularly with low photon counts systems such as in rapid, live cell imaging. This is becoming increasingly demanding with the development of novel CMOS SPAD array based widefield FLIM systems, which can generate significant volumes of data [9-11]. In this paper we present a new, rapid and robust method of extracting lifetime information that requires no prior information on the lifetime components.

There are different FLIM algorithms, mainly in two categories, the time domain (TD) and frequency domain (FD) approaches. FD FLIM mostly uses intensified CCDs synchronized to a modulated excitation source for widefield imaging [12-15]. The acquisition time is typically a few seconds, but fitting methods are required to extract the lifetimes which can take several seconds to minutes depending on the accuracy requirements. FD lifetime analysis software are usually iterative based. Furthermore accuracy is limited by the CCD array modulation, with the number of phase images (the time bins) typically between 2 to 20. For the TD systems, on the other hand, a pulsed laser is typically used in conjunction with a single photon counting detector, such as a PMT or SPAD Typical TD FLIM instruments either use 1) a time-correlated single-photon counting (TCSPC) module or 2) a time-gated CCD or SPAD [1, 9, 16]. For a TCSPC system, the measurements of the time delay between the laser pulses and the detected photon are repeated, and a histogram of time delays is accumulated in which the lifetimes are extracted using fitting algorithms [17]. TCSPC has been the gold standard FLIM technique due to its high timing resolution (typically < 100 ps), and recent developments in multi-channel TCSPC systems [18-20] further allow much faster acquisition, but the increased data

Manuscript received February 17, 2015; revised Xxx xx, 2015; accepted Xxx xx, 2015. Date of publication Xxx xx, 2015; date of current version Xxx xx, 2015. This work was supported by the China Scholarship Council (CSC), Royal Society (RG140915), the Medical Research Council (MRC: MR/K01563X/1, MR/K015664/1), the Biological Sciences Research Council (BBSRC: BB/K016865/1). *Asterisk indicates corresponding author*.

*Hq. Yu is with the School of Electronic Science and Engineering, National University of Defence Technology, Changsha 410073, China, and Centre for Biophotonics, Strathclyde Institute of Pharmacy & Biomedical Sciences, University of Strathclyde, Glasgow, G4 0RE, UK (e-mail: 13755132901@163.com).

Rebecca Saleeb and Paul Dalgarno are with The Institute of Biological Chemistry, Biophysics and Bioengineering, The School of Engineering & Physical Sciences; Heriot-Watt University, Edinburgh, EH14 4AS, UK (e-mail: rss31@hw.ac.uk; P.A.Dalgarno@hw.ac.uk)

$David Day-Uei Li is with Centre for Biophotonics, Strathclyde Institute of Pharmacy & Biomedical Sciences, University of Strathclyde, Glasgow, G4 0RE, UK (e-mail: david.li@strath.ac.uk).

Color versions of one or more of the figures in this paper are available online at http://ieeexplore.ieee.org.
Digital Object Identifier xx.xxxx/TBME.xxxx.xxxxxxx.

throughput accordingly demands faster fitting strategies [21]. For a time-gated camera, a series of intensity images at different delays are recorded to extract lifetimes. Similar to TCSPC systems, curve-fitting software are used to calculated lifetimes when the number of gates is larger than 5. The limitations of either FLIM systems are robust and rapid lifetime extractions. This work aims to provide rapid lifetime extractions from the lowest photon signal data possible (highest noise) to enable increasingly rapid imaging solutions.

There are two kind of algorithms mainly employed to obtain accurate fluorescence lifetimes. The first type is the widely used fitting methods, including Bayesian [22], maximum likelihood or maximum entropy [23], method of moments [24-26] and promptness ratio method [27]. Although fitting methods are precise, they are limiting as 1) they are computationally intensive, 2) they require prior information about how many lifetime components are contained in the data and therefore model selection is required, and 3) they easily converge to local minima. For realistic experiments, particularly in the low photon regime, it may be difficult to precisely know how many lifetime exponents are in every pixel, and researchers usually need to try or choose a proper data model for accurate fitting. The second method for extracting lifetimes are the non-fitting methods, including the phasor algorithm [28, 29], Prony's method [30], the integral equation method (IEM) [31], the center-of-mass method (CMM) [32-35], rapid lifetime determination (RLD) [36-39]. The phasor method and Prony's method are based on the first order model. The main criticism of all these techniques seems to be that they are all only good for mono-exponentials apart from phasor which may solve bi-exponentials if you know one component [40]. Gating techniques can be merged with iterative fitting techniques for resolving bi-exponential decays [27]. Kim *et al*. highlighted the limitations of traditional bi-exponential maximum-likelihood estimation (MLE) fitting and discussing proper gate width and how the IRF affects the estimations. This approach combined gating methods and MLE, and was only demonstrated on data sets of (τ_1, τ_2) = (1.0ns, 3,9 ns).

In this paper, we propose a new method of lifetime extraction based on a classical algorithm called estimation of signal parameters via rotational invariance techniques (ESPRIT) [22]. ESPRIT has been widely used in array signal processing for direction-of-arrival estimation of emitters, wireless communications, sonar and speech signal processing [41-43]. Inspired by ESPRIT, we proposed a new signal model and applied this model for estimation of fluorescence lifetime based on rotational invariance techniques, a system we term FLERIT. FLERIT is 1) non-iterative, 2) capable of resolving multi-exponential decays, 3) able to resolve lifetimes when the measurement-window-to-lifetime ratio is less than two and 4) suitable for implementations with embedded hardware for real-time applications. This paper presents the theory (section II), and demonstrates the potential through application to both simulated (section III) and experimental (section IV) data.

II. THEORY

Similar to previously published literature, we suppose the number of the exponential decays is P without considering the instrumental response function (IRF) [44]. Following the model proposed by Hall and Selinger [24], the fluorescence intensity density can be expressed in continuous time domain as

$$y(t)=\sum_{j=1}^{P}\left(f_{Dj}e^{-t/\tau_j}\right)+n(t),$$

where f_{Dj} and τ_j are the coefficient and the lifetime of the j-th decay component respectively, and $n(t)$ is the shot noise. The i-th bin of the TCSPC histogram is

$$y(i)=\sum_{j=1}^{P}\left(f_{Dj}e^{-ih/\tau_j}\right)+n(i)$$

where h is the timing resolution of the TCSPC system.

To reduce the computational complexity and noise, we merged B consecutive bins in the original histogram to create a new histogram with K bins as shown in Fig. 1. The histogram in Fig. 1(a) may be obtained by a TCSPC, whereas the one in Fig. 1(b) is obtained by a time-gated FLIM instrument. The photon count in the i-th bin of the new histogram is

$$x(i)=\sum_{l=1}^{B}y\left((i-1)B+l\right),i=1,\ 2,\ 3,\ldots,K\ .$$

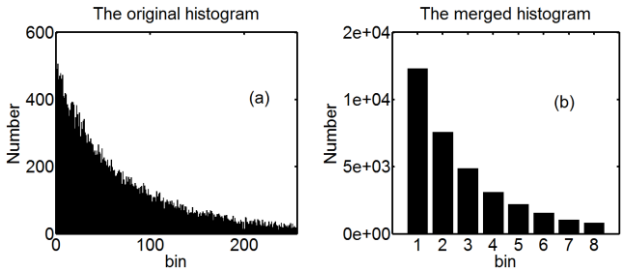

Fig. 1. (a) Original histogram and (b) merged histogram (K = 8).

We can arrange the counts from all time bins in the merged histogram as mentioned in [45] as

$$X=\left(x(1),x(2),\cdots,x(K)\right)^T$$

$$=\left(\sum_{l=1}^{B}y(l),\sum_{l=B+1}^{2B}y(l),\cdots,\sum_{l=(K-1)B+1}^{KB}y(l)\right)^T$$

$$=\begin{pmatrix} Q_1 & Q_2 & \cdots & Q_P \\ Q_1e^{-\frac{Bh}{\tau_1}} & Q_2e^{-\frac{Bh}{\tau_2}} & \cdots & Q_Pe^{-\frac{Bh}{\tau_P}} \\ \vdots & \vdots & \ddots & \vdots \\ Q_1e^{-\frac{(K-1)Bh}{\tau_1}} & Q_2e^{-\frac{(K-1)Bh}{\tau_2}} & \cdots & Q_Pe^{-\frac{(K-1)Bh}{\tau_P}} \end{pmatrix}\begin{pmatrix} f_{D1} \\ f_{D2} \\ \vdots \\ f_{DP} \end{pmatrix}+\begin{pmatrix} m(1) \\ m(2) \\ \vdots \\ m(K) \end{pmatrix}, \quad (1)$$

where

$$m(i)=\sum_{l=1}^{B}n\left((i-1)B+l\right),$$

and

$$Q_j=e^{-h/\tau_j}\left(1-e^{-Bh/\tau_j}\right)/\left(1-e^{-h/\tau_j}\right),\ j=1,\ldots,P\ .$$

For simplicity, rewrite (1) as

$$X = AS + M . \quad (2)$$

The covariance matrix of (2)[46] can be obtained as

$$R_X = E\left[XX^H\right] = AR_S A^H + \sigma^2 I , \quad (3)$$

where $(\cdot)^H$ represents the Hermitian transpose and

$$R_S = E\left[SS^H\right].$$

Applying SVD decomposition to R_X, we have

$$R_X = \begin{bmatrix} U_S & U_N \end{bmatrix} \begin{bmatrix} \Sigma_S & O \\ O & \sigma^2 I \end{bmatrix} \begin{bmatrix} U_S^H \\ U_N^H \end{bmatrix} = U_S \Sigma_S U_S^H + \sigma^2 U_N U_N^H . \quad (4)$$

As $U_N U_N^H + U_S U_S^H = I$ (U_S contains P eigenvectors corresponding to the P largest eigenvalues of R_X), we can obtain

$$U_S = AR_S A^H U_S \left(\Sigma_S - \sigma^2 I\right)^{-1} = AD \quad (5)$$

where D is a $P \times P$ non-singular matrix.

Rewriting the right-handed side of (5) as

$$AD = \begin{bmatrix} A_1 D \\ C_1 D \end{bmatrix} = \begin{bmatrix} C_2 D \\ A_2 D \end{bmatrix}, \quad (6)$$

where C_1 is the last row of A with the dimension $1 \times P$, C_2 is the first row of A with the dimension $1 \times P$, and the dimension of the A_1 and A_2 is $(K-1) \times P$, it is easily seen that the relationship between A_1 and A_2 is

$$A_2 = A_1 \Phi , \quad (7)$$

where

$$\Phi = diag\left(e^{-h/\tau_1}, \cdots, e^{-h/\tau_P}\right). \quad (8)$$

Equation 8 shows that all the fluorescence lifetimes are included in the eigenvalues of the matrix Φ. Therefore, once the eigenvalues $\lambda_j, j = 1, \ldots, P$, are obtained, all lifetimes can be calculated accordingly by

$$\tau_j = h / \ln\left(\lambda_j\right), j = 1, \ldots, P . \quad (9)$$

Similarly, the left-handed side of (5) can be arranged as

$$U_S = \begin{bmatrix} U_1 \\ U_3 \end{bmatrix} = \begin{bmatrix} U_4 \\ U_2 \end{bmatrix}. \quad (10)$$

where U_3 is the last row of U_S with the dimension $1 \times P$, U_4 is the first row of U_S with the dimension $1 \times P$, and the dimension of the U_1 and U_2 is $(K-1) \times P$.

From (5) (6) (7), we have

$$U_1 = A_1 D ,$$
$$U_2 = A_2 D = A_1 \Phi D ,$$

so

$$U_1 D^{-1} \Phi D = A_1 D U_1 D^{-1} \Phi D = A_1 \Phi D = U_2 .$$

Let

$$\Psi = D^{-1} \Phi D , \quad (11)$$

then

$$U_1 \Psi = U_2 . \quad (12)$$

From (11), the eigenvalues of Ψ are equivalent to those of Φ according to the similarity transformation rule [46].

We can calculate Ψ from (12) by applying LU factorization [46] and its eigenvalues $\lambda_j, (j = 1, \ldots, P)$, by SVD decomposition. The lifetimes can be estimated accordingly by (9). Finally, we can use the following equation to estimate $f_{Dj}, j = 1, \ldots, P$, from

$$S = (A^H A)^{(-1)} A^H X . \quad (13)$$

The above outlines the derivation of FLERIT, which can summarize to:

Step 1: Reduce the original histogram into K bins;

Step 2: calculate the correlation matrix of the new histogram using the covariance matrix (3);

Step 3: apply SVD decomposition to R_X, (4), to obtain the signal subspace U_S;

Step 4: obtain Ψ from (10) and (12);

Step 5: calculate the eigenvalues of Ψ by SVD decomposition;

Step 6: obtain the lifetimes by (9) and f_{Dj}, by (13).

The computational burden of the FLERIT is mainly from the SVD decomposition, which is about $O(K^3)$.

III. Simulations on Single-Exponential Decays

We compared the proposed FLERIT with IEM, CMM and Phasor in terms of A) lifetime dynamic range, B) photon efficiency, and (C) K using Monte-Carlo simulations for single-exponential decays. The F-value is the normalized precision defined as $F = \sqrt{N_C} \cdot \sigma_\tau / \tau$ [47] (F = 1 for the ideal case, and F > 1 or F >> 1 for realistic FLIM algorithms), where N_C is the number of all photons in the histogram and τ the calculated lifetime. To run the simulations, we assume there are 1024 time bins in a histogram and the measurement window T = 12.5ns. The analysis will allow us to optimize the performances of FLERIT.

A. Dynamic Range

We set K = 8 and the photon number in the first bin is 1000. Fig. 2(a) and (b) show the normalized bias ($\Delta\tau / \tau$) and F-value, respectively, in terms of the lifetime. Simulations show that FLERIT has the lowest bias among the four methods. Although CMM shows the lowest F-value with the best photon efficiency, its bias is significant when τ> 3ns and a bias correction measure is required to reduce the bias [35]. IEM has the least optimized range in bias. Phasor shows much less efficient when τ > 3ns. The optimized region (F < 4) is from 0.4 to 14ns for FLERIT, 0.4 to 8.8ns for IEM, and 0.4ns to 4.23ns ns for Phasor.

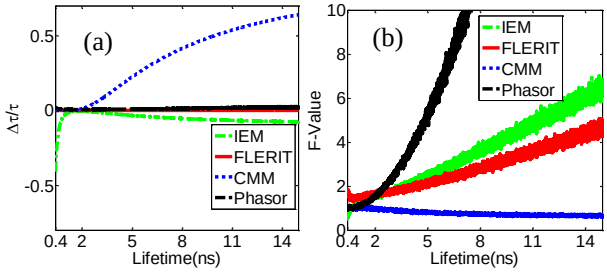

Fig. 2. (a) Bias and (b) F-value plots for different methods in terms of τ (0.4~15ns). K = 8, T = 12.5ns, the photon number in the first bin is 1000, and the number of the time bins is 1024.

B. *Photon Efficiency*

The normalized bias and *F*-value plots in terms of the photon count in the first bin (100~5000) for different methods are shown in Fig. 3(a) and (b). Here we use K = 8 and τ = 3ns. Again, FLERIT shows the lowest bias. It is interesting that the *F*-value of FLERIT is similar to IEM, larger than CMM and less than Phasor. But CMM has the worst bias performance, unless a bias correction is carried out. Figure 3(a) shows that both the bias and the normalized *F*-value should be independent of the photon count as expected.

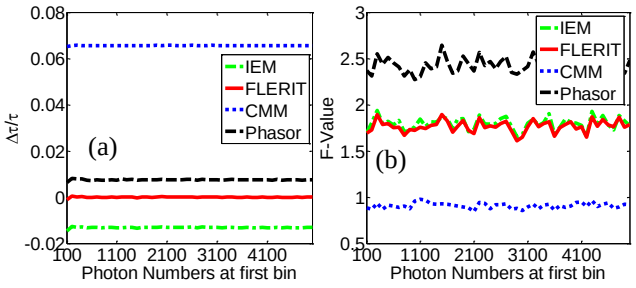

Fig. 3. (a) Bias, (b) *F*-value plots for different methods in terms of the photon count. K = 8, τ = 3ns, and the number of the time bins before merging is 1024.

C. *Performances in terms of* K

The normalized bias and *F*-value plots in terms of K ($4 < K < 32$) for different methods are shown in Fig. 4(a) and (b). Here we set τ = 3ns, the photon number in the first bin is 1000, and the number of the time bins is 1024. For FLIRET, the *F*-value degrades as K increases. FLERIT has similar bias performances with IEM, whereas Phasor and CMM are significantly biased. Figure 4(a) shows that Phasor and CMM favor a larger *K*. This means FLERIT can be used to resolve histograms obtained by gated FLIM systems as well as TCSPC systems.

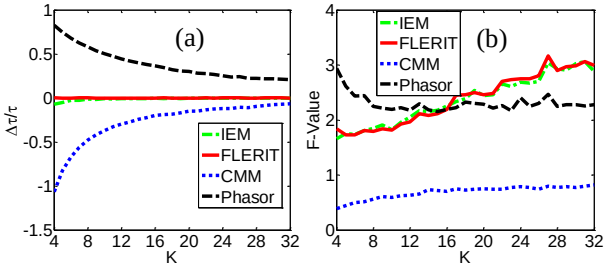

Fig. 4. (a) Bias, (b) *F*-value plots for different methods in terms of K. τ = 3ns, the photon number in the first bin is 1000, number of time bins before merging is 1024.

IV. Lifetime Resolvability Analysis

To test whether FLERIT can resolve bi-exponential decays robustly, Monte Carlo simulations were carried out with τ_1 = 1.5ns, 1.5ns < τ_2 < 6ns, (f_{D1}, f_{D2}) = (0.5, 0.5), M = 1024, and 100 < N_c < 100000. Other simulation settings are the same as Fig. 2. The histogram was merged into a new one with K = 8. The probability of successfully resolving τ_1 and τ_2, $P_{Correct}$, is defined as the number of correct estimations (the normalized bias is less than 50%) to the number of total simulations. The simulation results are shown in Fig. 5. Simulations show that

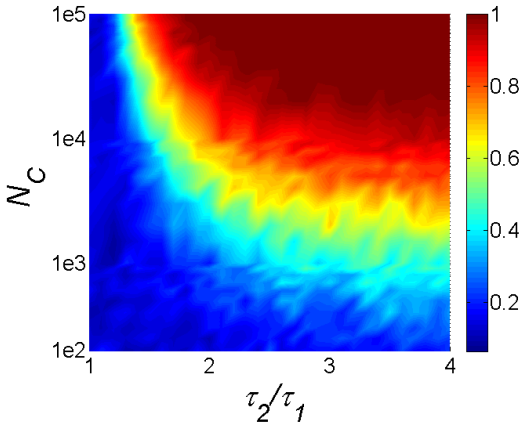

Fig.5 Probability of resolving τ_1 and τ_2, τ_1 = 1.5ns, 1.5ns < τ_2 < 6ns, $(f_{D1}, f_{D2}) = (0.5, 0.5)$ and other settings are same as Fig. 3.

$P_{Correct}$ is a function of N_c and τ_2 / τ_1. Simulations show that FLERIT is unable to resolve lifetimes when τ_2 / τ_1 < 1.4. Figure 5 also shows that the threshold of N_c is about 10000.

V. Analysis on Synthesized Multi-decay FLIM Data

In TCSPC FLIM experiments the photons collected at each image pixel is limited, either due to the time taken to obtain a viable histogram, limiting for live cell imaging, or due to photobleaching. Pixel binning is therefore often applied to improve the signal-to-noise (SNR) of FLIM images at the sacrifice of spatial resolution. To illustrate the FLERIT methodology and advantages, we first use synthesized data with the number of photons limited both A) without and B) with pixel binning.

A. *Without pixel binning*

When there is only one lifetime, the number of eigenvectors of the signal space U_S is one. However, an interesting feature found in FLERIT is that when there are multiple lifetimes, the eigenvector corresponding to the biggest eigenvalue of R_X is actually a linear combination of all lifetimes when the photon count is limited, i.e. $\tau = f_{D1}\tau_1 + f_{D2}\tau_2 + \cdots$. In Fig. 6(a), assume the histogram in each area is $y(t) = f_{D1}e^{-t/\tau_1} + f_{D2}e^{-t/\tau_2} + \cdots$. The laser repetition rate is set to be 80MHz (T = 12.5ns).

In the first simulated case we define the primary and secondary lifetimes τ_1 = 2ns and τ_2 = 5ns for all areas and (f_{D1}, f_{D2}) = (0.8, 0.2), (0.5, 0.5), and (0.2, 0.8) for areas *A*, *B*, and *C*, respectively. The image size is 256×256 pixels. The photon count at the first bin is 500, and the number of time bins in the histogram is 256 (the histogram was merged into a new one with K = 8). The photon count (intensity) of the original data is shown as Fig. 6(a).The averaged lifetime image obtained by FLERIT is shown as Fig. 6(b).

This article has been accepted for publication in a future issue of this journal, but has not been fully edited. Content may change prior to final publication. Citation information: DOI 10.1109/TBME.2015.2491364, IEEE Transactions on Biomedical Engineering

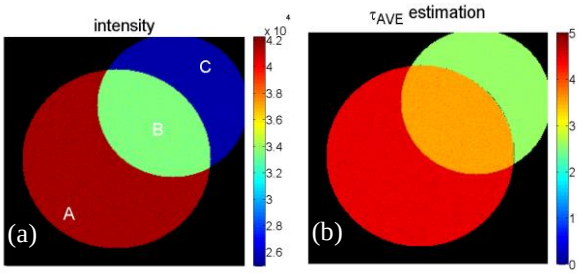

Fig. 6. (a) The intensity and (b) average lifetime image for synthesized data. τ_1 = 2ns; τ_2 = 5ns; (f_{D1}, f_{D2}) = (0.8, 0.2), (0.5, 0.5), and (0.2, 0.8) for areas *A*, *B*, and *C*, respectively. The image size is 256×256 pixels.

The mean (τ_{AVE}), standard deviation and *F*-value (normalized precision; F = 1 for the ideal case, and $F > 1$ or $F >> 1$ for realistic FLIM algorithms) of the calculated lifetimes for the three areas are listed in Table I. The precision of the average lifetime is similar to the single-exponential case in Section III.

TABLE I
PERFORMANCES OF FLERIT WITHOUT PIXEL BINNING.

Area	Exact average lifetime (ns)	Calculated parameters		
		mean (ns)	Standard deviation (ns)	*F* value
Area *A*	4.4	4.45	0.06	1.40
Area *B*	3.5	3.53	0.05	1.43
Area *C*	2.6	2.58	0.03	1.94

Consider the second case of a tri-exponential decay where τ_1 = 2ns; τ_2 = 3ns; τ_3 = 5ns; f_{D1} = 0.4, 0.33, and 0.2, f_{D2} = 0.4, 0.33, and 0.2, f_{D3} = 0.2, 0.34, and 0.6, for the areas *A*, *B*, and *C*, respectively. The photon count (intensity) of the original data is shown as Fig. 7(a).The averaged lifetime image obtained by FLERIT is shown as Fig. 7(b).

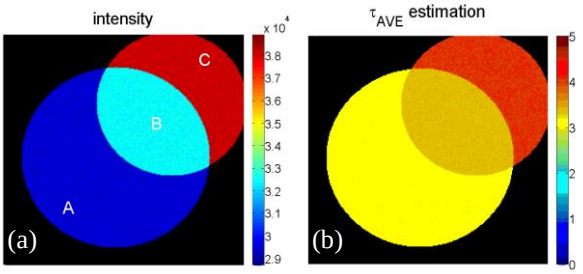

Fig. 7. (a) The intensity and (b) average lifetime image for synthesized tri-exponential decays. A tri-exponential decay where τ_1 = 2ns; τ_2 = 3ns; τ_3 = 5ns; f_{D1} = 0.4, 0.33, and 0.2, f_{D2} = 0.4, 0.33, and 0.2, f_{D3} = 0.2, 0.34, and 0.6, for the areas *A*, *B*, and *C*, respectively.

TABLE II
PERFORMANCES OF FLERIT FOR SYNTHESIZED TRI-EXPONENTIAL DECAYS.

Area	Real average lifetime (ns)	Calculated parameters		
		mean (ns)	Standard deviation (ns)	*F* value
Area *A*	3	3.00	0.04	2.06
Area *B*	3.35	3.36	0.04	2.22
Area *C*	4	4.03	0.05	2.55

Tables I and II confirm that FLERIT offers an interesting feature similar to the previously reported IEM [33] when it deals with multi-exponentials:

$$\tau_{AVE} = \sum_{j=1}^{P} f_{Dj}\tau_j \,. \qquad (14)$$

This is a useful feature, as in some applications such as FRET-FLIM experiments [7], (11) can be used to estimate the FRET efficiency. In many biological applications however, it is desirable to estimate τ_j and f_{Dj}, $j = 1,\ldots,P$ and as previously discussed IEM is only a single exponential approximation.

B. With pixel binning:

Due to limited photons in the histogram, it is challenging to estimate f_{D1} accurately using (13). Typically pixel binning is used to increase the photon count by trading off the spatial resolution. Using the synthesized data presented in Fig. 6, we adopted a summation based binning procedure as shown in Fig. 8. The intensity after binning is shown in Fig. 8(a). After binning, τ_1, τ_2, f_{D1} and f_{D2} can be estimated, and the averaged lifetime can be calculated as shown in Fig. 9(b) using (14).

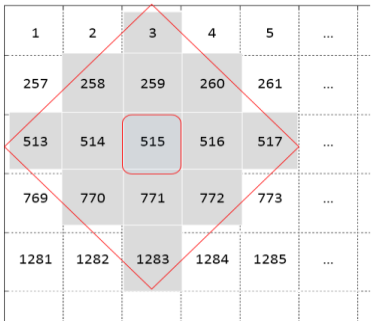

Fig. 8. The binning strategy. The binned data in the square is summed up by all the data in the diamond.

The performances including the mean, standard deviation and *F*-value of calculated parameters are listed in Table III. The table contains more parameters than Table II, as FLERIT resolves all lifetime components and proportional coefficients. The *F*-value is slightly worse than that in Table I, but the FLERIT conducts a blind bi-exponential analysis solving all four parameters (τ_1, τ_2, f_{D1} and f_{D2}). The photon efficiency for obtaining the same precision in the *F*-value is 26-fold better if an experiment only requires τ_{AVE} [31] (For some applications it is not essential to resolve all τ_j and f_{Dj}).

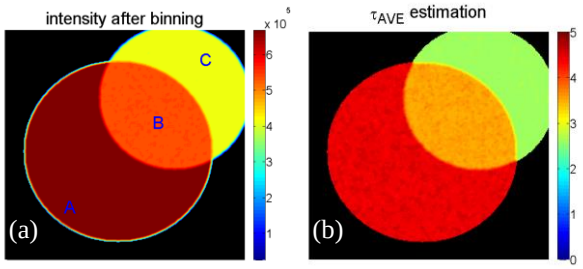

Fig. 9. (a) The intensity and (b) the average fluorescence lifetime images after binning. The simulation setting is the same as Fig. 6.

Fig. 10(a) and (b) depict τ_1 and τ_2 images, respectively. When f_{Dj} is higher, the standard deviation of the corresponding lifetime is lower. Similar to other methods, when f_{D1} approaches 0.0 or 1.0 (nearly single-exponential), it requires much more photons to obtain accurate τ_1 and τ_2, respectively.

This article has been accepted for publication in a future issue of this journal, but has not been fully edited. Content may change prior to final publication. Citation information: DOI 10.1109/TBME.2015.2491364, IEEE Transactions on Biomedical Engineering

Fig. 11(a) shows the f_{D1} image after binning. Fig.11 (b) shows lifetime histograms for τ_1, τ_2 and τ_{AVE}. The peak of τ_1 and τ_2 is around 2.01ns and 4.94ns, in good agreement with the exact values. The calculated τ_{AVE} are 2.60ns, 3.51ns and 4.41ns, again close to the theoretical τ_{AVE} 2.6ns, 3.5ns, 4.4ns in areas *B*, *C* and *A* as shown in Fig. 6(a). The SNR of τ_{AVE} is much better than each individual τ_j and f_{Dj}. The ratio of the measurement window to τ_2 (12.5ns/5ns), is only 2.5, much smaller than the recently proposed bi-exponential algorithms [48], indicating that the duty cycle of the laser repetition can be higher giving better photon efficiency.

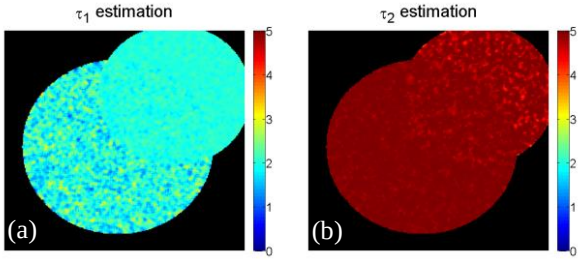

Fig.10 (a) τ_1 and (b) τ_2 images binning. The simulation setting is the same as Fig. 6.

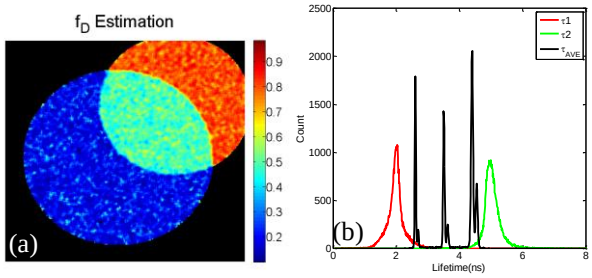

Fig. 11. (a) f_D image and (b) lifetime histograms for τ_1, τ_2 and τ_{AVE} after binning. The simulation setting is the same as Fig. 6.

TABLE III
PERFORMANCES OF FLERIT ON BI-EXPONENTIAL DATA AFTER BINNING.

Item	Exact value	Simulation results		
		mean	Standard deviation	*F* value
τ_{AVE} of area *A*	4.4ns	4.40 ns	0.05 ns	2.24
τ_{AVE} of area *B*	3.5 ns	3.52 ns	0.07 ns	3.51
τ_{AVE} of area C	2.6ns	2.62 ns	0.05 ns	3.05
f_{D1} estimation of area *A*	0.2	0.21	0.07	-
f_{D1} estimation of area *B*	0.5	0.49	0.05	-
f_{D1} estimation of area *C*	0.8	0.79	0.04	-
τ_1 estimation (all A, B, C)	2 ns	1.99 ns	0.46 ns	-
τ_2 estimation (all A, B, C)	5 ns	5.03 ns	0.96 ns	-
τ_1 estimation of area *A*	2 ns	1.99 ns	0.39 ns	-
τ_1 estimation of area *B*	2 ns	2.00 ns	0.14 ns	-
τ_1 estimation of area *C*	2 ns	1.99 ns	0.07 ns	-
τ_2 estimation of area *A*	5 ns	5.02 ns	0.19 ns	-
τ_2 estimation of area *B*	5 ns	5.02 ns	0.21 ns	-
τ_2 estimation of area *C*	5 ns	5.02 ns	0.42 ns	-

VI. EXPERIMENTS

To test FLERIT on real data, FLIM experiments were carried out on HeLa cells ubiquitously expressing EGFP using a commercial scanning confocal FLIM system

A. Experimental set up

Data was acquired using a Leica SP5 scanning confocal microscope fitted with a PicoHarp 300 TCSPC module. Excitation was with a tunable white light laser (WLL) operating at 488 nm and 40 MHz. Detection was with a single channel MPD SPAD, collecting the majority of EGFP emission. All images where Nyquist sampled, 512x512 pixels and with predefined total image integration times set to 10s, 60s, 180s and 600s.

B. Sample preparation

HeLa cells were plated onto 25mm glass coverslips previously coated with 50ug/ml poly-D-Lysine hydrobromide (UV irradiated for sterility) and grown for 24 hours at 37ºC and 5% CO_2. Cells were cultured in DMEM (Gibco, 31053) supplemented with 100U/ml penicillin, 100ug/ml streptomycin (Gibco, 15140), 10% heat-inactivated foetal bovine serum (Gibco, 10500064), 1X Glutamax (Gibco, 35050) and 1mM sodium pyruvate (Gibco, 11360). Following 24 hour growth, cells were transfected using Turbofect transfection reagent (Thermo Scientific, R0531) with 2ug pEGFP-N1, a discontinued Clontech plasmid encoding enhanced green fluorescent protein, and incubated for a further 24 hours at 37ºC and 5% CO_2 to allow expression of the encoded EGFP. Cells were washed with 1X phosphate buffered saline, fixed with 4% paraformaldehyde and blocked with 50mM ammonium chloride prior to mounting on slides with MOWIOL 4-88 and allowing to set overnight before imaging.

C. Experiment data analysis

Fig. 12 shows the epifluorescence image an example cell with ubiquitously expressed EGFP. Fig. 13(a)-(d) show the average fluorescence lifetime image for the acquisition time of 10s, 60s, 180s, and 600s (the maximum photon count are 54, 251, 756, and 1939 respectively). The figures show that the deviations of the lifetime decrease as the acquisition time is increased. Fig. 14(a)-(d) show the histograms of τ_{AVE} for the acquisition time of 10s, 60s, 180s, and 600s. Figs. 14 show that the standard deviation can be improved with a longer acquisition and it is inversely proportional to the square root of the acquisition, in agreement with the conclusion given in [28]. Fig. 15(a)-(d) show the histograms of τ_1 and τ_2 for different acquisitions. The bi-exponential ingredient is 1.58%, 2.12%,

This article has been accepted for publication in a future issue of this journal, but has not been fully edited. Content may change prior to final publication. Citation information: DOI 10.1109/TBME.2015.2491364, IEEE Transactions on Biomedical Engineering

2.12% and 2.21% respectively for 10s, 60s, 180s, and 600s. The peaks of τ_1 and τ_2 histograms are located at around 850ps and 3ns. The average lifetime is about 2.8ns, in accordance with Ref [49].

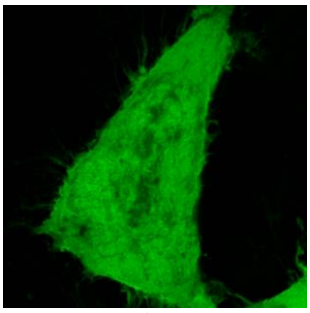

Fig. 12. The epifluorescence image.

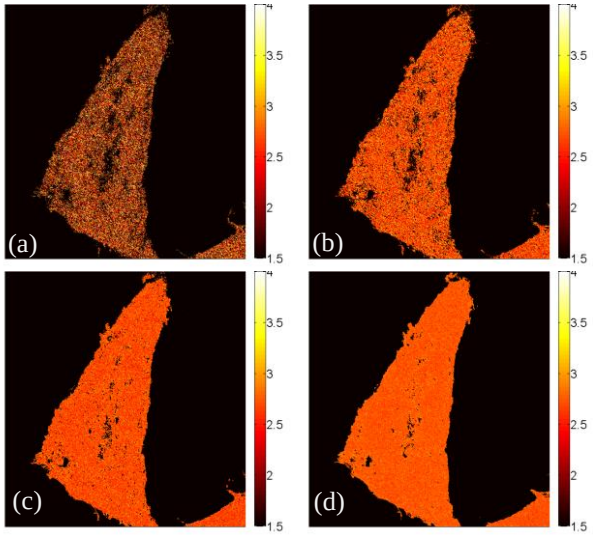

Fig. 13. τ_{AVE} images for the acquisition of (a) 10s, (b) 60s, (c) 180s and (d) 600s.

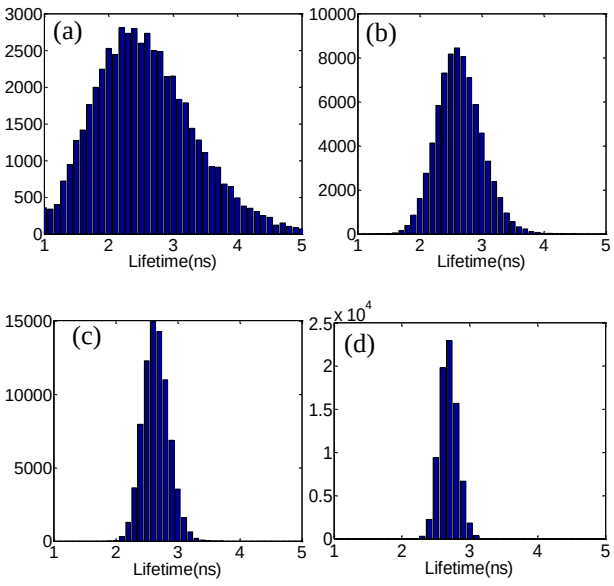

Fig. 14. τ_{AVE} histograms for the acquisition of (a) 10s, (b) 60s, (c) 180s and (d) 600s.

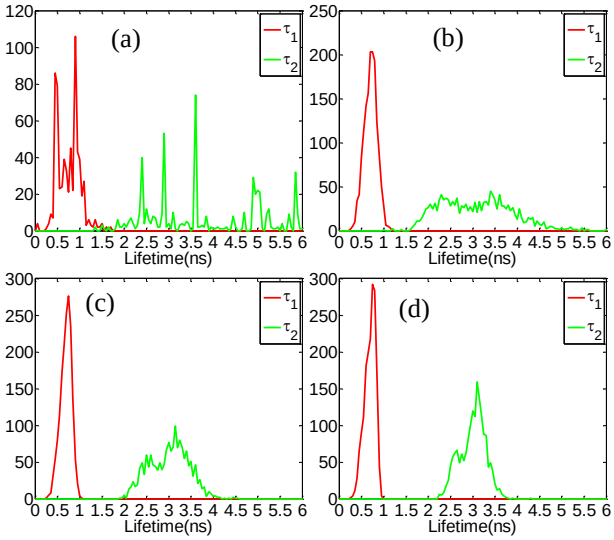

Fig. 15. τ_1 and τ_2 histograms of for the acquisition of (a) 10s, (b) 60s, (c) 180s and (d) 600s.

D. Time consumption of the data analysis

We have run the data analysis using MATLAB® on DELL Optiplex 7010 desktop. For a 512x512 image, it takes 26.7s. If FLERIT is implemented in a hardware similar to Ref. [31], the computational burden can be further decreased by adopting fast multistage Wiener filtering method [50], Lanczos algorithm [51], and propagator method [52]. With more and more hardware multipliers or intellectual property cores embedded in DSP processors and FPGA circuits, the proposed method can be realized in such embedded systems for real-time applications.

VII. Conclusions

In this paper, we proposed a new method called FLERIT. The derivations of FLERIT have been carried out by introducing a signal model. The performances of FLERIT were demonstrated on both synthesized and experimental data. The new method does not require any prior information and it can be applied to both gated CCDs and TCSPC systems with limited number of timing channels. For more accurate analysis, the model can be extended to include the IRF, but it is an independent work not covered in this paper. Simulations and experiments show that FLERIT can provide single-exponential average fluorescence lifetimes similar to the previously reported IEM method or multiple exponential analysis. FLERIT can extract fluorescence lifetimes by only a few time gates, which can reduce the data throughput between a parallel TCPSC front-end and a data analyzing system. The computation burden of FLERIT is much less than traditional fitting methods making it suitable for implementations in embedded systems.

References

[1] M. Elangovan *et al.*, "Nanosecond fluorescence resonance energy transfer - fluorescence lifetime imaging microscopy to localize the protein interactions in a single living cell," *Journal of microscopy*, vol. 205, pp. 3-14, 2002.

[2] P. I. Bastiaens and A. Squire, "Fluorescence lifetime imaging microscopy: spatial resolution of biochemical processes in the cell," *Trends in cell biology*, vol. 9, pp. 48-52, 1999.

[3] S. Coda *et al.*, "Fluorescence lifetime spectroscopy of tissue autofluorescence in normal and diseased colon measured ex vivo using a fiber-optic probe," *Biomedical optics express*, vol. 5, pp. 515-538, 2014.

[4] T. S. Blacker *et al.*, "Separating NADH and NADPH fluorescence in live cells and tissues using FLIM," *Nature communications*, vol. 5, 2014.

[5] M. Nobis *et al.*, "Intravital FLIM-FRET imaging reveals dasatinib-induced spatial control of Src in pancreatic cancer," *Cancer research*, vol. 73, pp. 4674-4686, 2013.

[6] C. N. Medine *et al.*, "Munc18-1 prevents the formation of ectopic SNARE complexes in living cells," *Journal of cell science*, vol. 120, pp. 4407-4415, 2007.

[7] E. Fišerová and M. Kubala, "Mean fluorescence lifetime and its error," *Journal of Luminescence*, vol. 132, pp. 2059-2064, 8// 2012.

[8] T. Omer *et al.*, "Reduced temporal sampling effect on accuracy of time-domain fluorescence lifetime Förster resonance energy transfer," *Journal of biomedical optics*, vol. 19, pp. 086023-086023, 2014.

[9] S. Burri *et al.*, "Architecture and applications of a high resolution gated SPAD image sensor," *Optics Express*, vol. 22, pp. 17573-17589, 2014/07/14 2014.

[10] R. M. Field *et al.*, "A 100 fps, Time-Correlated Single-Photon-Counting-Based Fluorescence-Lifetime Imager in 130 nm CMOS," *Solid-State Circuits, IEEE Journal of*, vol. 49, pp. 867-880, 2014.

[11] C. Veerappan *et al.*, "A 160x128 single-photon image sensor with on-pixel 55ps 10b time-to-digital converter," in *Solid-State Circuits Conference Digest of Technical Papers (ISSCC), 2011 IEEE International*, 2011, pp. 312-314.

[12] L. Rosso and V. C. Fernicola, "Time- and frequency-domain analyses of fluorescence lifetime for temperature sensing," *Review of Scientific Instruments*, vol. 77, pp. 034901-034901-6, 2006.

[13] P. Roudot *et al.*, "Lifetime map reconstruction in frequency-domain fluorescence lifetime imaging microscopy," in *Image Processing (ICIP), 2012 19th IEEE International Conference on*, 2012, pp. 2537-2540.

[14] P. Vita *et al.*, "Deep-ultraviolet light-emitting diodes for frequency domain measurements of fluorescence lifetime in basic biofluorophores," *Applied Physics Letters*, vol. 87, pp. 084106-084106-3, 2005.

[15] M. Zhao *et al.*, "Parallel excitation-emission multiplexed fluorescence lifetime confocal microscopy for live cell imaging," *Optics Express*, vol. 22, pp. 10221-10232, 2014/05/05 2014.

[16] H. Yu and D. D.-U. Li, "Fluorescence lifetime extraction algorithm based on multiple signal classification," *Electronics Letters*, vol. 51, pp. 81-83, 2015.

[17] L. Turgeman and D. Fixler, "Photon Efficiency Optimization in Time-Correlated Single Photon Counting Technique for Fluorescence Lifetime Imaging Systems," *Biomedical Engineering, IEEE Transactions on*, vol. 60, pp. 1571-1579, 2013.

[18] S. P. Poland *et al.*, "A high speed multifocal multiphoton fluorescence lifetime imaging microscope for live-cell FRET imaging," *Biomedical Optics Express*, vol. 6, pp. 277-296, 2015/02/01 2015.

[19] J. F. Hauer *et al.*, "Initial results in Prony analysis of power system response signals," *Power Systems, IEEE Transactions on*, vol. 5, pp. 80-89, 1990.

[20] J. L. Rinnenthal *et al.*, "Parallelized TCSPC for Dynamic Intravital Fluorescence Lifetime Imaging: Quantifying Neuronal Dysfunction in Neuroinflammation," *PLoS ONE*, vol. 8, p. e60100, 2013.

[21] S. P. Poland *et al.*, "Time-resolved multifocal multiphoton microscope for high speed FRET imaging in vivo," *Optics Letters*, vol. 39, pp. 6013-6016, 2014.

[22] M. I. Rowley *et al.*, *Bayesian analysis of fluorescence lifetime imaging data* vol. 7903, 2011.

[23] R. Swaminathan and N. Periasamy, "Analysis of fluorescence decay by the maximum entropy method: Influence of noise and analysis parameters on the width of the distribution of lifetimes," *Proceedings of the Indian Academy of Sciences - Chemical Sciences*, vol. 108, pp. 39-49, 1996/02/01 1996.

[24] P. Hall and B. Selinger, "Better estimates of exponential decay parameters," *The Journal of Physical Chemistry*, vol. 85, pp. 2941-2946, 1981/10/01 1981.

[25] M. Maus *et al.*, "An Experimental Comparison of the Maximum Likelihood Estimation and Nonlinear Least-Squares Fluorescence Lifetime Analysis of Single Molecules," *Analytical Chemistry*, vol. 73, pp. 2078-2086, 2001/05/01 2001.

[26] S. Pelet *et al.*, "A fast global fitting algorithm for fluorescence lifetime imaging microscopy based on image segmentation," *Biophysical journal*, vol. 87, pp. 2807-2817, 2004.

[27] G.-H. Kim *et al.*, "Single-Molecule Analysis And Lifetime Estimates Of Heterogeneous Low-Count-Rate Time-Correlated Fluorescence Data," *Applied spectroscopy*, vol. 65, pp. 981-990, 2011.

[28] S. Zahner *et al.*, "Fluorescence lifetime imaging microscopy and polar-plot analysis of gallium selenide crystals," *Journal of Applied Physics*, vol. 115, pp. 043504-043504-7, 2014.

[29] A. Leray *et al.*, "Three-dimensional polar representation for multispectral fluorescence lifetime imaging microscopy," *Cytometry Part A*, vol. 75A, pp. 1007-1014, 2009.

[30] Z. Zhang *et al.*, "Prony's method for exponential lifetime estimations in fluorescence‐based thermometers," *Review of Scientific Instruments*, vol. 67, pp. 2590-2594, 1996.

[31] D.-U. Li *et al.*, "Real-time fluorescence lifetime imaging system with a 32x32 0.13μm CMOS low dark-count single-photon avalanche diode array,"

Optics Express, vol. 18, pp. 10257-10269, 2010/05/10 2010.

[32] D. D. U. Li *et al.*, "Video-rate fluorescence lifetime imaging camera with CMOS single-photon avalanche diode arrays and high-speed imaging algorithm," *Journal of Biomedical Optics,* vol. 16, pp. 096012-096012-12, 2011.

[33] D. D.-U. Li *et al.*, "Time-Domain Fluorescence Lifetime Imaging Techniques Suitable for Solid-State Imaging Sensor Arrays," *Sensors,* vol. 12, pp. 5650-5669, 2012.

[34] P. R. Barber *et al.*, "Global and pixel kinetic data analysis for FRET detection by multi-photon time-domain FLIM," in *Proc. SPIE 5700*, 2005, pp. 171-181.

[35] D.-U. Li *et al.*, "Hardware implementation algorithm and error analysis of high-speed fluorescence lifetime sensing systems using center-of-mass method," *Journal of Biomedical Optics,* vol. 15, pp. 017006-017006-10, 2010.

[36] D. M. Grant *et al.*, "High speed optically sectioned fluorescence lifetime imaging permits study of live cell signaling events," *Optics Express,* vol. 15, pp. 15656-15673, 2007/11/26 2007.

[37] R. M. Ballew and J. N. Demas, "An error analysis of the rapid lifetime determination method for the evaluation of single exponential decays," *Analytical Chemistry,* vol. 61, pp. 30-33, 1989/01/01 1989.

[38] R. Woods *et al.*, "Transient digitizer for the determination of microsecond luminescence lifetimes," *Analytical chemistry,* vol. 56, pp. 1395-1400, 1984.

[39] S. P. Chan *et al.*, "Optimized gating scheme for rapid lifetime determinations of single-exponential luminescence lifetimes," *Analytical chemistry,* vol. 73, pp. 4486-4490, 2001.

[40] A. Leray *et al.*, "827Spatio-Temporal Quantification of FRET in Living Cells by Fast Time-Domain FLIM: A Comparative Study of Non-Fitting Methods," *PLoS ONE,* vol. 8, p. e69335, 2013.

[41] G. Mao *et al.*, "Wireless sensor network localization techniques," *Computer networks,* vol. 51, pp. 2529-2553, 2007.

[42] H. Kim and M. Viberg, "Two decades of array signal processing research," *IEEE signal magazine,* vol. 13, pp. 67-94, 1996.

[43] D. L. Hall and J. Llinas, "An introduction to multisensor data fusion," *Proceedings of the IEEE,* vol. 85, pp. 6-23, 1997.

[44] E. G. Novikov *et al.*, "Linear algorithms for stretched exponential decay analysis," *Optics communications,* vol. 166, pp. 189-198, 1999.

[45] M. Y. Berezin and S. Achilefu, "Fluorescence lifetime measurements and biological imaging," *Chemical reviews,* vol. 110, pp. 2641-2684, 2010.

[46] R. A. Horn and C. R. Johnson, *Matrix analysis*: Cambridge university press, 2012.

[47] H. C. Gerritsen *et al.*, "Fluorescence lifetime imaging in scanning microscopes: acquisition speed, photon economy and lifetime resolution," *Journal of Microscopy,* vol. 206, pp. 218-224, 2002.

[48] D. D.-U. Li *et al.*, "Fast bi-exponential fluorescence lifetime imaging analysis methods," *Optics Letters,* vol. 40, pp. 336-339, 2015/02/01 2015.

[49] G. Striker *et al.*, "Photochromicity and fluorescence lifetimes of green fluorescent protein," *The Journal of Physical Chemistry B,* vol. 103, pp. 8612-8617, 1999.

[50] J. S. Goldstein *et al.*, "A multistage representation of the Wiener filter based on orthogonal projections," *Information Theory, IEEE Transactions on,* vol. 44, pp. 2943-2959, 1998.

[51] Z. Bai, "Krylov subspace techniques for reduced-order modeling of large-scale dynamical systems," *Applied Numerical Mathematics,* vol. 43, pp. 9-44, 2002.

[52] S. Marcos *et al.*, "The propagator method for source bearing estimation," *Signal processing,* vol. 42, pp. 121-138, 1995.